CHAPTER: VI

SYNERGISTIC EFFECT OF GRAPHENE OXIDE ON THE PROPERTIES OF POLY (VINYL ALCOHOL)/CARBOXYMETHYL CELLULOSE ELECTRO SPUN NANOFIBER MATS

6.1 Introduction

In the contemporary world, nanotechnology is rapidly advancing, driven by its capacity to create innovative materials that are applicable across various processes [1]. Researchers are actively engaged in studying polymer nanocomposites due to enhanced properties of nanomaterials, as well as advancing in nanofiber development [2]. Nanofibers generated through diverse manufacturing techniques find extensive applications, especially in packaging, energy storage, air and water purification filters, and membrane technologies etc [3,4]. Different techniques have been developed for generating nanofibers, such as melt blowing, bicomponent fiber splitting, phase separation, dry-wet spinning, centrifugal spinning, self-assembly, and electrospinning etc [5]. Among different techniques, electrospinning stands as a simple, cost-effective, and easily accessible approach for the development of nanofibers [6]. It has proven effective in generating more than a hundred distinct types of nanofibers from polymers and their blends, featuring diameters spanning from a few nanometres to several hundred microns [7]. Moreover, it provides the ability to control the shape, alignment, and nanofiber dimensions by adjusting parameters such as applied voltage, flow rate, distance between the jet and collector, temperature, and humidity in the manufacturing process [8–10]. However, with proper adjustments to the processing parameters, it is possible to produce uniform and bead-free nanofibers with diameters that meet specific requirements. Electrospun nanofibers possess a high aspect ratio, large specific surface area, with excellent physiochemical properties, while maintaining stability under high temperatures. Due to these unique features, nanofiber membranes are emerging as a promising innovation in food packaging with broad potential applications. These membranes are typically made from polymers that offer a combination of desirable characteristics, including flexibility, pleasant texture, breathability, biodegradability, and

durability. The high surface area-to-volume ratio and porous structure of membrane make them ideal for controlled release of active ingredients [11]. One of the key advantages of electrospun nanofiber mats is their excellent barrier properties. This feature enhances the sealing of food packaging, reduces permeability, and effectively inhibits microbial growth. Furthermore, these mats can selectively filter gases such as oxygen and carbon dioxide, forming a natural controlled atmosphere that helps preserve the freshness of fruits and vegetables [12].

Thus, the study focuses on the development and characterization of nanofiber mats by PVA, PVA/CMC, and PVA/CMC/GO polymeric solutions. The impact of additives, specifically CMC biopolymer and GO nanofiller, on solution properties such as viscosity, conductivity, and rheology has been examined. Additionally, the nanofiber mats were analyzed to assess how these additives influence their physicochemical, mechanical, thermal, and barrier properties. The experimental findings were compared with previous studies to provide a comprehensive understanding of the research and highlight its potential applications in the packaging biomedical industries.

6.2 Preparation of polymer solutions for electrospinning

The details of the materials and reagents used for the development of films has been stated detailed in Chapter 3, under the materials and methodology section 3.1. Previous studies have shown that PVA concentrations between 6 wt.%-10 wt.% produces smooth, bead-free nanofibers by electrospinning. Therefore, for the present study, minimum PVA concentration of 6 wt.% was used as the base polymer solution for electrospinning. For developing PVA/CMC hybrid polymer solutions, different concentrations of CMC 0.5 wt.%-1.5 wt.% was considered in polymer solution ratio of (1:1) as shown in Table 1. Moreover, for the development of PVA/CMC/GO polymer solution, 0.1 wt.%-0.5 wt.% GO was used as an additive. Initially, 6% (w/v) of PVA (i.e. 6g of PVA dissolved in 100 ml distilled water) was dissolved in distilled water and stirred on a magnetic stirrer at 90 °C and 600 rpm for 3 hours to ensure homogeneous mixing. The PVA solution was then mixed with 1% (v/v) glycerol and 2% v/v $CaCl_2$ (i.e. 1 ml of glycerol and 2ml of calcium chloride mixed in the PVA solution), and the stirring continued for 30 min, followed by sonication for complete removal of bubbles [13,14]. To develop PVA/CMC blended polymer solution, different concentrations of CMC were considered and the procedure for the development of CMC solution is stated in reference [15] Afterwards, PVA and CMC solutions was taken 1:1 ratio in a beaker and stirred on a magnetic stirrer at 600 rpm for 3

hours. The blended PVA/CMC solution was then sonicated to remove bubbles present in the solution. In the case of the PVA/CMC/GO polymer solution, different concentrations of GO (0.1 wt.%-0.3 wt.%) were added to the hybrid PVA/CMC blended polymer mixture and stirred until a uniform distribution of GO was achieved. The solution was then sonicated for 15 min for bubble free solution and homogeneous mixing of GO nanofiller within the solution. The developed solutions were then further used for electrospinning.

6.3 Fabrication of nanofiber mats

The fabrication of nanofiber mats was performed in ESPIN Nano equipment. The polymer solutions prepared from all the combinations of polymer and GO nanofiller has been mentioned in Table 6.1.

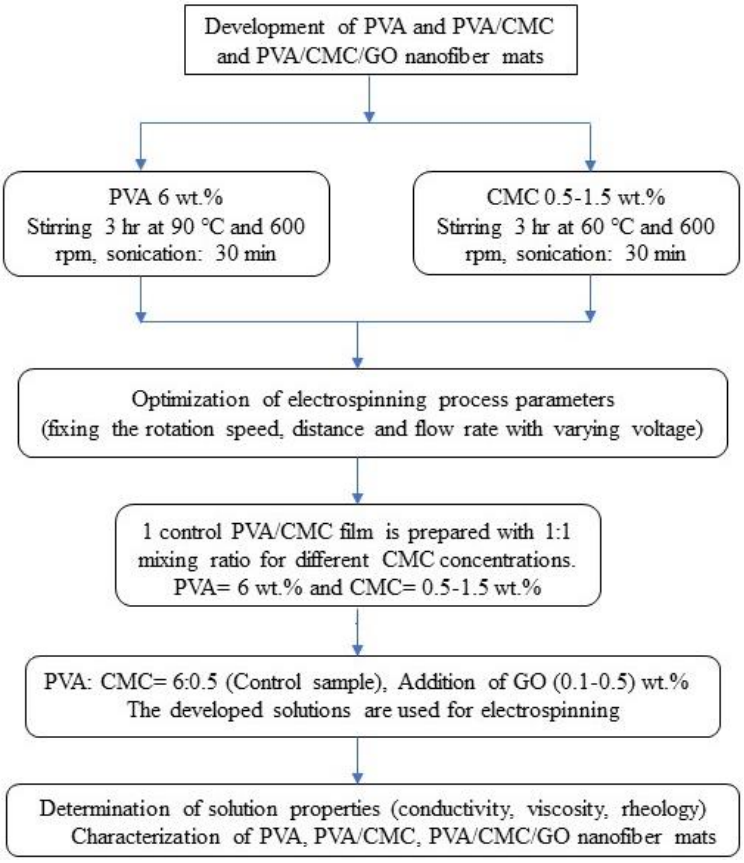

Figure 6.1 Flowchart of experimental procedure for the development of nanofiber mats

The polymer solution was loaded into a 10 ml needle-tip syringe with a 22 mm gauge needle, positioned at a specific distance of 15 cm from the drum collector (rotational speed: 900 rpm) and with a flow rate of 0.3 mL/h. Nanofibers were deposited onto aluminium foil above the drum collector, and the resulting nanofiber mats was dried for 24 hours at 45 °C in a hot air oven [16].

To develop nanofiber mats from the polymer solutions, various electrospinning process parameters were performed, as outlined in Table 6.1. The electrospin process was performed by fixing the rotation speed, distance and flow rate while the voltage was varied from 15 kV to 30 kV for all the solutions. Table 6.1 indicates that no nanofiber formation was observed in the samples $P_6C_{1.5}$, P_6C_1 and $P_6C_{0.5}G_{0.5}$ solutions at different process parameters. However, the remaining solutions P_6, $P_6C_{0.5}$, $P_6C_{0.5}G_{0.1}$, and $P_6C_{0.5}G_{0.5}$ were successfully electrospun at 25 kV. A schematic illustration for the preparation of nanofiber solution and development of nanofiber mats has been shown in Figure 6.1 and Figure 6.2.

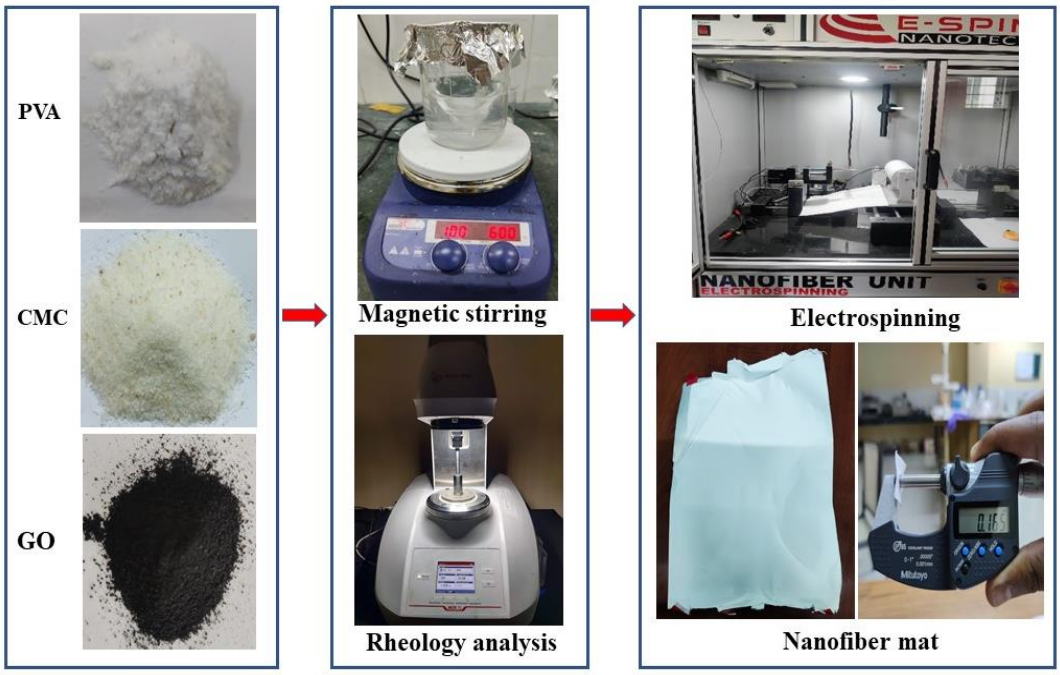

Figure 6.2 Schematic illustration for the development of nanofiber mats

For the production of control PVA/CMC hybrid nanofiber mats, different concentrations of CMC (ranging from 0.5 wt.% to 1.5 wt.%) were used in 1:1 polymer solution ratio. However, as the CMC concentrations exceeds 0.5 wt.%, it was challenging for the electrospinning jet to generate nanofibers due to increase in viscosity of the solution. This impends the solution's ability to elongate under the electric field's forces, resulting in an unstable electrospinning jet and leading to unsuccessful fiber production. Thus, the optimum concentration of PVA and CMC for the development of control nanofiber mat in the ratio 1:1 were 6 wt.% and 0.5 wt.%.

For the fabrication of GO induced PVA/CMC nanofiber mats, GO (0.1 wt.%-0.5 wt.%) were considered, as shown in Table 6.1. Based on experimental trials it was established that the concentration of GO was limited to 0.3 wt.%. Higher concentrations of

GO were challenging for the formation of nanofibers during the electrospinning process due to increase in agglomeration of GO and higher solution viscosity, leading to difficulties in maintaining a stable jet necessary for nanofiber formation. This limitation was even observed consistently across different processing parameters tested, confirming that nanofibers was not successfully produced at concentrations exceeding 0.3 wt.%. Thus, the polymer solution prepared from P_6, $P_6C_{0.5}$, $P_6C_{0.5}G_{0.1}$, and $P_6C_{0.5}G_{0.5}$ were successfully electrospun and selected for further characterizations.

Table 6.1 Electro spin process parameters

Polymer solutions ratio (1:1) Composition (w/v)		Nano Filler (%wt.)	Samples name	Rotation speed (rpm)	Tip collector distance (cm)	Accelerating Voltage (kV)	Nanofiber formation
PVA	CMC	GO					
6	1.5	-	$P_6C_{1.5}$	900	15	15-30	No
6	1	-	P_6C_1	900	15	15-30	No
6	-	-	P_6	900	15	25	Yes
6	0.5	-	$P_6C_{0.5}$	900	15	25	Yes
6	0.5	0.1	$P_6C_{0.5}G_{0.1}$	900	15	25	Yes
6	0.5	0.3	$P_6C_{0.5}G_{0.3}$	900	15	25	Yes
6	0.5	0.5	$P_6C_{0.5}G_{0.5}$	900	15	15-30	No

6.4 Results and discussion

6.4.1 Conductivity and viscosity

The solution properties of the above selected polymer composition were examined and displayed in Figure 6.3. In electrospinning, solution parameters (i.e. concentration, viscosity, and molecular weight, surface tension, conductivity) and processing parameters (i.e. applied voltage, flow rate, temperature and humidity) are important parameters in determining nanofiber diameter [1]. For sample P_6, the solution conductivity was found to be 24.91×10^{-3} S/m. However, with the addition of Na-CMC the conductivity of the blended $P_6C_{0.5}$ solution was increased significantly to 102.58×10^{-3} S/m. Adding CMC to the polymer solution releases sodium ions (Na^+), thus enhancing the charge carrier density and overall conductivity. CMC disrupts the crystalline structure of PVA, creating an amorphous phase that increases ionic transport and further improves conductivity. Research shows that solution parameters play a crucial role in determining nanofiber diameter. In particular, higher solution conductivity leads to a reduction in fiber diameter, while an increase in fiber

diameter is controlled by the higher viscosity of the polymer solution [5,17]. Thus, conductivity appears to be the dominating factor in contributing to the reduction in nanofiber diameter from 116.27±37.64 nm to 90.51±17.56 nm (P_6 to $P_6C_{0.5}$) as evident in Figure 6.7 FESEM micrographs. Addition of GO from 0.1% to 0.3% ($P_6C_{0.5}G_{0.1}$-$P_6C_{0.5}G_{0.3}$) resulted in a marginal enhancement in conductivity from 106.75×10^{-3} S/m to 107.58 ×10^{-3} S/m. This suggests that the charge carrier density and mobility were marginally increased at the indicated GO loadings, probably due to agglomeration.

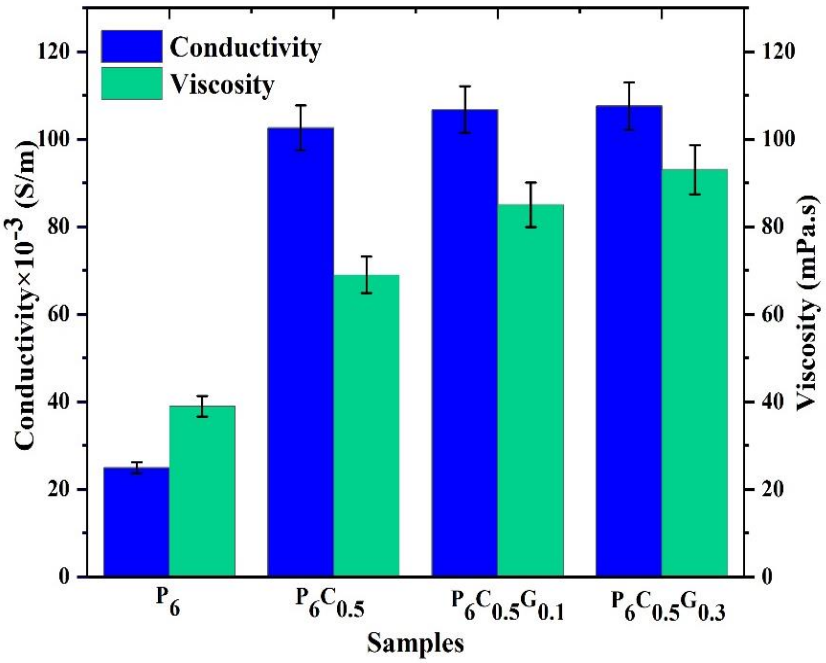

Figure 6.3 Polymer solution conductivity and viscosity

The viscosity of the polymer solution, is one of the key factors for nanofiber fabrication, as higher viscosity hinders the smooth flow of the polymer through the electrospinning needle [18]. From Figure 6.3, it was observed that the viscosity of sample P_6 and $P_6C_{0.5}$ were 39 mPa.s and 69 mPa.s respectively. The alteration in viscosity with the addition of CMC improved the flow properties of $P_6C_{0.5}$ solution, thus enabling consistent nanofiber production under the same electrospinning conditions. Hence, 6% PVA and 0.5% CMC in a polymer mixing ratio of 1:1 showed uniform nanofiber formation without clogging of polymer in the electrospinning needle. In line with existing literature, successful nanofiber development was observed at 2% CMC concentration across all ratios except for 50/50 ratio [18]. Similar results were reported with the increase in solution viscosity of pure starch and PVA polymer with the addition of 0.4 % CMC [19].

With the addition of GO from 0.1 wt.%-0.3 wt.%, a significant increment in the

solution viscosity from 85 mPa.s to 93 mPa.s was observed. The substantial increment in viscosity was due to higher solid content in the polymer solution as well as modified interactions between polymer chains and GO sheets. The change in solution viscosity led to increase in fiber diameters from 134.81±31.10 nm to 169.22±73.54 nm ($P_6C_{0.5}G_{0.1}$-$P_6C_{0.5}G_{0.3}$) as observed in the FESEM micrographs in Figure 6.7. Different concentrations of GO ranging from 0.1 wt.% to 0.5 wt.% were considered for the development of nanofiber mats as shown in Table 6.1. However, it was difficult to develop nanofiber with concentrations exceeding 0.3 wt.% due to the elevated solution viscosity, which hindered smooth spinning of the solution. Similar results were reported in terms of increase in nanofiber diameter for PVA/GNS-H and Ni-YSZ nanofibers [20,21].

6.4.2. Rheology analysis

6.4.2.1. Storage modulus and loss modulus vs angular frequency

The flow characteristics of film-forming solution plays a crucial role in determining the spreadability, coating layer thickness, uniformity, mechanical properties, overall design, application, and processing [22]. Hence, conducting a comprehensive examination on the rheological characteristics of polymer-based solutions is imperative. Dynamic frequency sweeps were carried out to comprehend the viscous and elastic characteristics of film forming solutions, as shown in Figure 6.4.

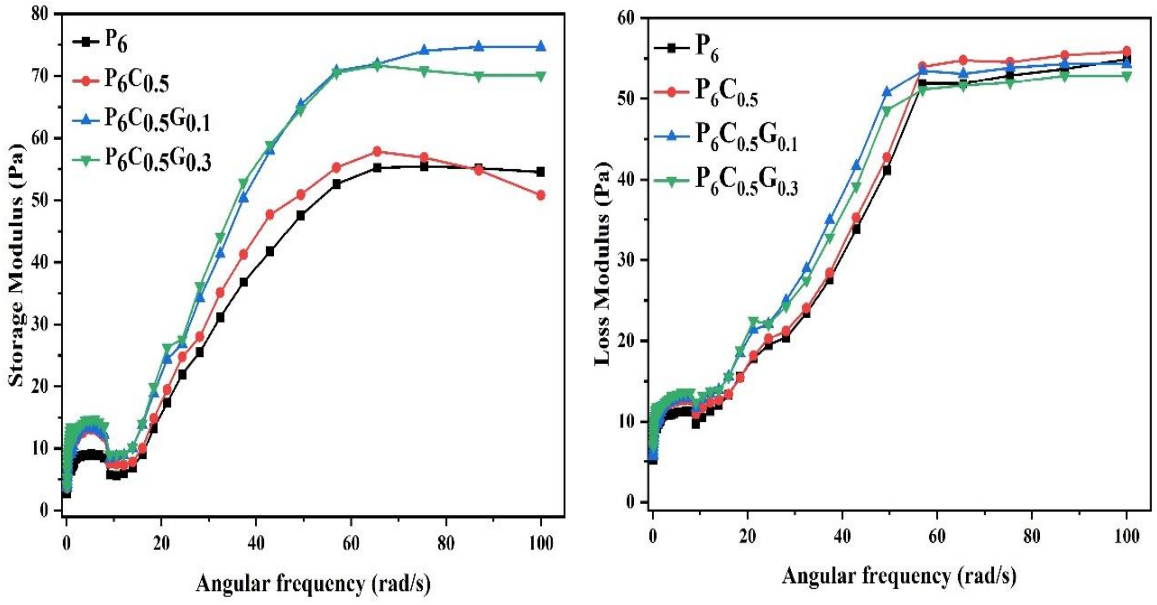

Figure 6.4 Storage modulus (G′), loss modulus (G″) vs angular frequency

The data set demonstrates G′ (storage modulus), representing elastic behaviour, and G″ (loss modulus), indicating viscous behaviour [23]. The data indicates that nanofiber solutions primarily exhibit viscous behaviour at low frequencies, where G" is less than G', and elastic behaviour at high frequencies, where G' becomes more significant than G". The values of G″ from samples (P_6 to $P_6C_{0.5}G_{0.3}$) in the frequency range of 0-10 rad/s varied from 10.50 Pa to 13.17 Pa, whereas G′ values ranged from 5.61 Pa to 9.03 Pa. At lower frequencies, the G″ value was higher than G′ for sample $P_6C_{0.5}G_{0.3}$, followed by $P_6C_{0.5}G_{0.1}$ and $P_6C_{0.5}$, indicating solution's viscous characteristics. As the frequency sweep was enhanced from 20-30 rad/s, a distinctive shift in the viscoelastic properties of the samples was observed at the crossover point, indicating a characteristic change toward elastic behaviour. In higher frequency range up to 100 rad/s, the G′ recorded for samples P_6 and $P_6C_{0.5}$ was 54.52 Pa and 50.81 Pa, while their G″ was 54.89 Pa and 55.87 Pa, respectively. Hence, it was evident that blending PVA with CMC makes the interaction of the negatively charged carboxylate group in CMC with the polar -OH groups in PVA. This enhanced the crosslinking between the two polymers, resulting in the creation of a hybrid polymer matrix that is more stable and cohesive compared to single polymer system.

With the addition of 0.1 wt.%-0.3 wt.% GO, the values of G′ for samples $P_6C_{0.5}G_{0.1}$ and $P_6C_{0.5}G_{0.3}$ was 74.68 Pa and 70.10 Pa, while G″ was 54.30 Pa and 52.87 Pa, respectively. The enhanced elastic response of the material is attributed to the exceptional mechanical properties of the GO nanofiller. The combination of PVA and CMC creates an exfoliated network that triggers the shifts between flexible and stiff states when GO is introduced. The functional groups in GO improves the distribution of nanoparticles in the polymer solution, changing the phase transitions, while providing durability and stiffness [24]. Moreover, the coherent increase in G′ upon incorporating GO attributed to the strong molecular forces and interaction between the OH group and the epoxide linkage of GO, signifying an enhancement in load-bearing properties [25,26]. Similar results were reported with the increase in storage modulus at higher concentration of graphene [27].

6.4.2.2 Viscosity vs shear rate

The changes in viscosity of the polymer solution with respect to shear rate are depicted in Figure 6.5. It was observed that the apparent viscosity of P_6 solution increases with the increase in the shear rate and then levels off, indicating the shear-thickening properties of the solution. The shear-thickening phenomenon is associated with the alterations in the macromolecular structure caused by flow properties, along with the

deformation and interactions of macromolecules [28]. At lower shear rates, the macromolecule structural transformation occurs through polymer chain rearrangement via intermolecular interactions, leading to an increase in the solution viscosity, and such a trend is associated with non-Newtonian dilatant fluids [29]. Similar results were reported for aqueous PVA solution under different shear rates thus validating the present study [28,30].

With the addition of CMC, a similar behaviour of apparent viscosity was observed, indicating the shear-thickening of the $P_6C_{0.5}$ blend as seen in Figure 6.5. The apparent viscosity of the blended solution was significantly higher at a lower shear rate compared to PVA solution. The rise in apparent viscosity while increasing shear rate was due to the development of intramolecular forces between carboxylate and hydroxyl groups of CMCs and PVA which alters the solution viscosity [30,31]. Thus, addition of CMC influences the relationship between viscosity and shear rate, extending the after-flow phase.

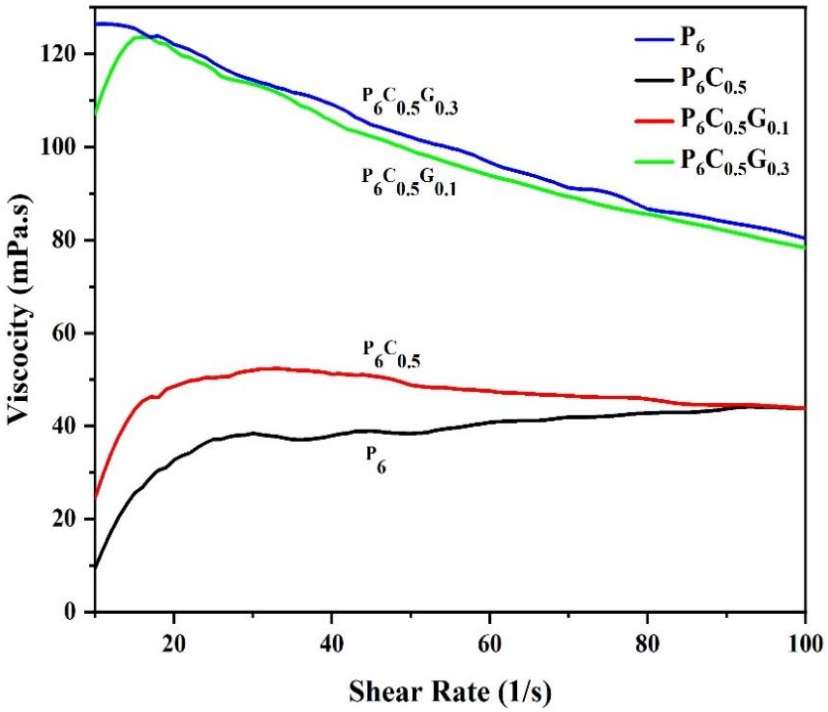

Figure 6.5 Viscosity vs shear rate

A significant change in apparent viscosity was also observed while adding GO nanofillers in PVA/CMC solution as depicted in Figure 6.5. The reduction in viscosity with increasing shear rate confirmed solution's shear thinning (pseudoplastic) behaviour. The shear-thinning behavior is linked to the robust entanglement of GO within the PVA/CMC polymer solution. In the strong thinning region, the flow characteristics of the suspensions

closely resembles to PVA/CMC solution, suggesting primary mechanism involving the disruption of the H-bond. This underscores an extra thinning mechanism related to the flow-induced alignment of GO nanosheets at high aspect ratio. At zero shear rate, nanoparticles arranged randomly in liquid suspension due to the lack of intermolecular interactions [32]. However, applying shear the polymeric chain leads to uniform alignment in the flow direction, decreasing viscosity at higher shear rates. Adding GO into the liquid suspension induces a significant elastic response due to the interactions between nanoparticles and the polymeric chain. The degree of entanglement between polymeric chains is affected by the concentration of filler particles. Specifically, polymer chains near the nanoparticles become entangled or immobilized due to their proximity to the particles. At low filler concentrations, the uniform dispersion of nanofillers throughout the polymer matrix is characterized by significant interparticle spacing. A distinct interphase with minimal nanofiller concentrations embedded in the polymer matrix influences material's flow characteristics, potentially leading to alterations in the apparent viscosity of the nanocomposite solution as compared to the pure polymer solution [33]. Thus, the existence of GO within the polymer matrix significantly impacts the rheological characteristics, thereby affecting its processability, material's behaviour, and its properties.

6.4.2.3 Shear stress vs shear rate

The variations in shear stress with shear rate for PVA and its hybrid solutions are illustrated in Figure 6.6. The flow curves enable the categorization of film-forming solutions into Newtonian or non-Newtonian fluids. In the case of typical Newtonian fluids, the relationships between viscosity, shear stress, and shear rate are linear, with viscosity being independent of both shear rate and shear stress [34]. As depicted in Figure 6.6, a consistent increase in shear stress in the steady state was observed for PVA, PVA/CMC, and its nanocomposite with GO nanofillers. With increasing shear rate from 0 to 100 s^{-1}, linear variations in shear stress were found to be 0.07 to 4.38 Pa and 0.23 to 4.38 Pa for sample P_6 and $P_6C_{0.5}$ respectively. The addition of CMC alters the intermolecular forces in the PVA matrix, resulting in a more cohesive structure that can withstand shear stress. CMC serves as a thickening agent, raising the viscosity of the PVA solution which significantly improves the material's resistance to shear forces.

With the addition of 0.1-0.3% GO in the mixed polymer solution of PVA/CMC resulted in a significant increase in shear stress, ranging from (1.058 to 7.838) Pa and (1.26 to 8.03) Pa for $P_6C_{0.5}G_{0.1}$ and $P_6C_{0.5}G_{0.3}$, respectively. The enhancement in shear stress can

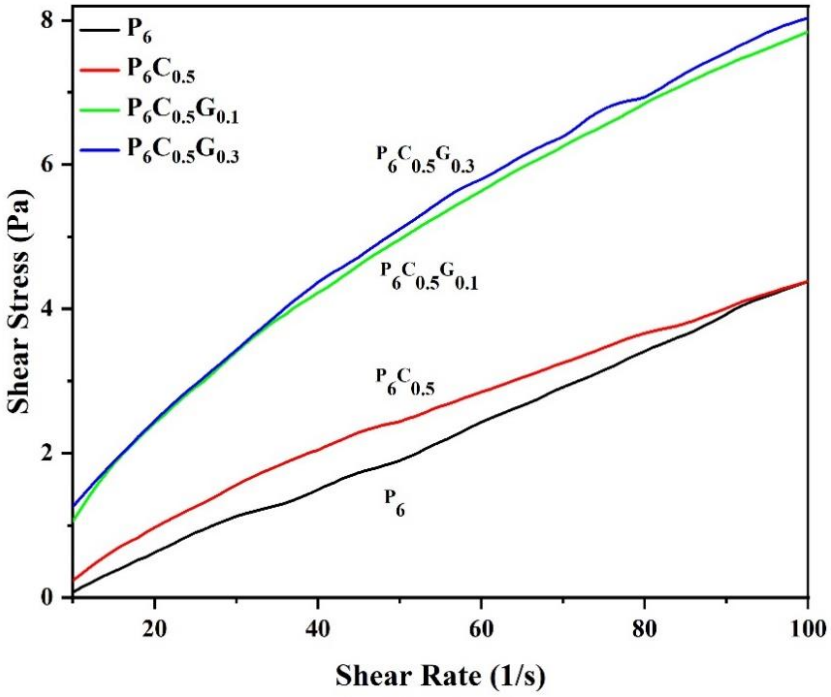

Figure 6.6 Shear stress vs shear rate

be ascribed to the oxygen functionalization of GO, which facilitates stronger non-covalent bonding within the polymer matrix [24]. The H-bond between GO and PVA/CMC polymer matrixes has been identified as an essential element for improving the modulus and stiffness of the polymer systems [5,35]. This phenomenon is particularly significant for polymers capable of acting as H-bond acceptors and donors. Covalent bonding between the filler and matrix represents an effective strategy to enhance interfacial shear stress for improved stress transfer. Thus, the findings hold promise for enhancing the rheological characteristics of PVA by incorporating CMC and GO nanofillers, making them applicable in engineering applications.

6.4.3 Morphology analysis

FESEM analysis was performed to investigate the morphological characteristics of the nanofiber mats, as illustrated in Figure 6.7(a) and its mean diameter distribution is illustrated in Figure 6.7(b). It was observed from the micrograph that pristine PVA nanofibers display smooth, regular, and bead-free structure with a mean diameter measuring approximately 116.27±37.64 nm. The micrograph of sample $P_6C_{0.5}$ also revealed smooth, bead-free structure, with an average diameter approximately 90.51±17.56 nm. Addition of CMC led to 28.46% decrease in the fiber diameter of $P_6C_{0.5}$ as compared to sample P_6. The reduction in fiber diameter is attributed to significant enhancement in

solution conductivity which leads to stronger electrostatic forces during the electrospinning process. Similar findings were reported regarding the reduction in fiber diameter with the rise in solution conductivity [5,35].

The FESEM micrographs of PVA/CMC/GO nanofibers, as seen in sample $P_6C_{0.5}G_{0.1}$ and $P_6C_{0.5}G_{0.3}$ displayed minimal bead formation and filler agglomeration, confirming successful dispersion of GO within the $P_6C_{0.5}$ polymer matrix. From sample $P_6C_{0.5}G_{0.1}$ to $P_6C_{0.5}G_{0.3}$, an increase in 25.50% of fiber diameter was observed with mean diameter ranged from 134.81±31.10 nm to 169.22±73.54 nm. The enhancement in fiber diameter upon the adding GO was due to the rise in solution viscosity. The reduction in fiber diameter from P_6 to $P_6C_{0.5}$ was due to the dominant factor of solution conductivity compared to viscosity. Whereas, significant increase in fiber diameter from $P_6C_{0.5}G_{0.1}$ to $P_6C_{0.5}G_{0.3}$ upon adding GO, was due to the significant enhancement in solution viscosity relative to its conductivity. As the solution viscosity increased, the polymer chains became more entangled, which sustain the continuity of the electrospinning jet and resulted in an increase in nanofiber diameter [36, 37].

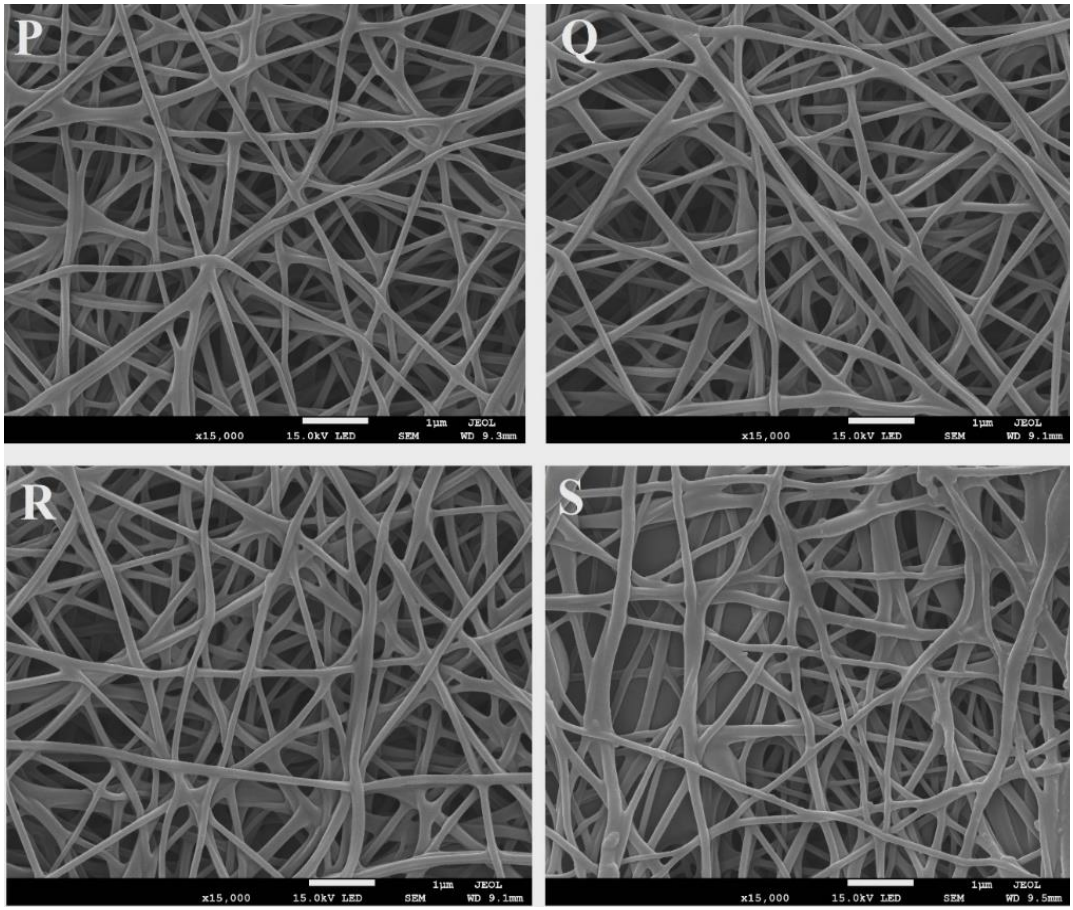

(a) FESEM micrographs (P: P_6; Q: $P_6C_{0.5}$; R: $P_6C_{0.5}G_{0.1}$; S: $P_6C_{0.5}G_{0.3}$)

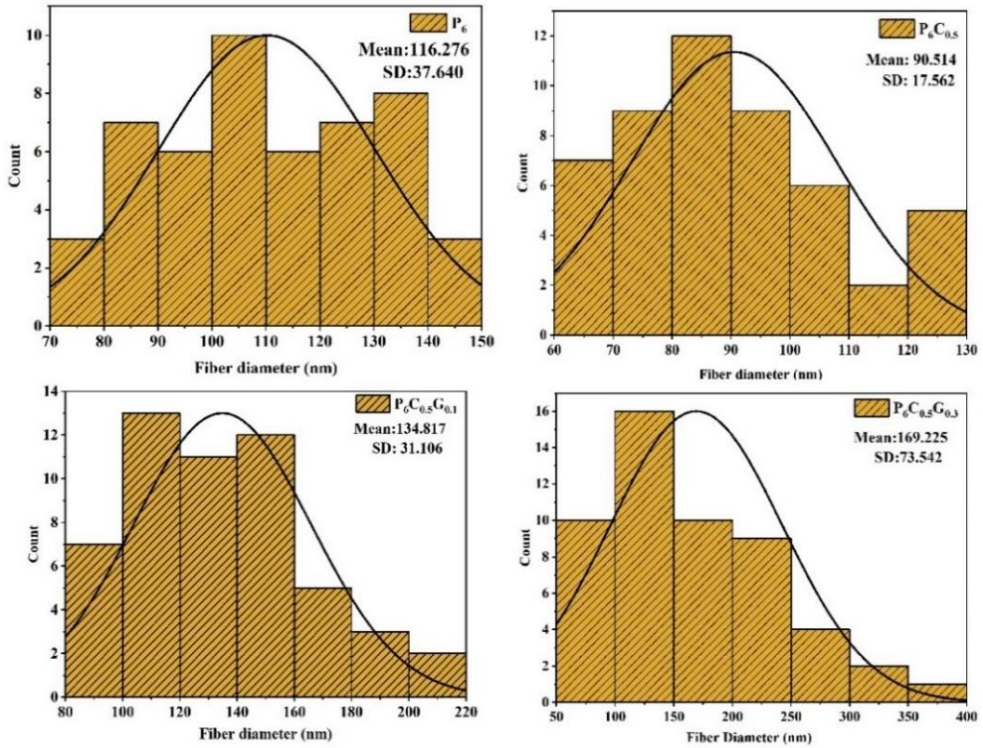

(b) Nanofiber diameter distribution

Figure 6.7 (a) FESEM micrographs and (b) nanofiber diameter distribution.

This observation aligns with earlier research demonstrating that adding graphene-based nanofillers led to thicker nanofibers [21]. The uniform surface morphology obtained suggests that graphene oxide (GO) was well-dispersed within the polymer matrix, likely due to the formation of hydrogen bonds between the GO surface and the PVA/CMC polymer chains. This indicates that GO was evenly integrated into the polymer system without significant aggregation or phase separation. The micrographs of $P_6C_{0.5}G_{0.1}$ and $P_6C_{0.5}G_{0.3}$ also revealed some protrusions in the nanofiber which is believed to be the GO sheets, displaying a spindle and irregular shape of fibers with GO particles extending from the smooth nanofiber surface. The formation of spherical bead-like nanofibers can also be attributed to the high boiling temperature, surface tension and viscosity of the polymer solution [38]. Thus, the morphological analysis revealed that the optimal ratios of CMC and GO substantially modify the diameters of the nanofibers, leading to improved surface characteristics for different applications.

The TEM images of PVA/CMC/GO films at concentrations of 0.1% and 0.3% are shown in Figure 6.8. Fiber network has been observed which shows GO interaction with the fibrous network or a part of fiber network of the nanocomposite. The interaction allows the network to maintain its integrity without significant clumping, thereby enhancing the mechanical strength and functional properties of the nanofiber mats [39]. Additionally,

the images also provide further evidence that the GO sheets have been successfully exfoliated within the polymer matrix, and the finding that is also supported by the FESEM images.

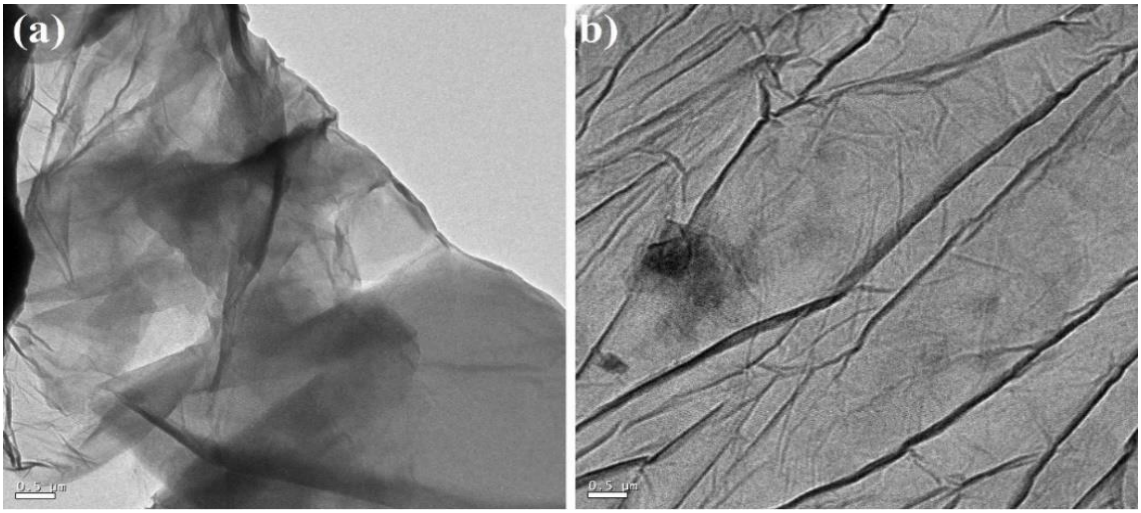

Figure 6.8 TEM image of PVA/CMC/GO (a) 0.1 wt.% of GO (b) 0.3 wt.% of GO

6.4.4 Thickness and tensile properties

The thickness, tensile strength (TS), and elongation at break (EAB) of the nanofiber mats are outlined in Table 6.2. It was observed that the thickness of the nanofiber mats ranged from 0.156 mm to 0.161 mm.

The TS and EAB of the pristine PVA nanofiber mats were found to be 11.36 MPa and 26.82%, respectively ($P \leq 0.05$). However, the inclusion of CMC resulted in significant increase in TS upto 13.49 MPa, and a decrease in EAB of up to 6.66%. The development of H-bond and enhanced cross-linked density within the nanofibers resulted in an 18.69% rise in TS and 75.14% decrease in elongation for $P_6C_{0.5}$ nanofiber mat compared to P_6. The development of a crystalline lattice structure within the composite is responsible for the material to become less elastic and more brittle. This, in turn, increases the stiffness and load-bearing capability of the nanofiber mat. Overall, the presence of CMC improves the mechanical properties of PVA nanofibers, making them suitable for various applications, including packaging and biomedical uses. A comparable pattern of elastic properties was noted where reduction in EAB from 22.27% to 18.91% with the addition of CMC [15]. As indicated in Table 6.2, adding 0.1 wt.%-0.3 wt.% GO sample $P_6C_{0.5}G_{0.1}$ to $P_6C_{0.5}G_{0.3}$ resulted in a notable increase in TS from 14.27 MPa to 16.64 MPa ($P \leq 0.05$). Compared to P_6, the TS was improved by 25.59% for sample $P_6C_{0.5}G_{0.1}$ and 46.41% for sample $P_6C_{0.5}G_{0.3}$. As compared to $P_6C_{0.5}$, the TS was improved by 5.81% for sample $P_6C_{0.5}G_{0.1}$

and 23.34% for sample $P_6C_{0.5}G_{0.3}$. The enhancements in TS was due to the uniform dispersion nature of GO and its good interfacial interaction with the polymer chain which subsequently increases nanofibers load transfer characteristics. However, the %EAB of samples $P_6C_{0.5}G_{0.1}$ and $P_6C_{0.5}G_{0.3}$ was 42.02% and 38.22%, respectively as seen in Table 6.2. The decrease in EAB and rise in TS observed at 0.3% GO concentration was due to the inclusion of solid nanoparticle, which makes the nanofiber mat brittle in nature, resulting in a decrease in EAB. Additionally, the presence of GO caused stress concentration due to the loose arrangement of nanofibers, further contributing to the reduction in %EAB [13,26]. The electrostatic forces in the electrospinning process played a key role in augmenting the interaction between PVA and GO nanofillers. Furthermore, the improved mechanical properties of GO-incorporated nanofiber mats were related to the optimal concentration of GO and its uniform dispersion, viscosity, solution conductivity, and processing parameters [40]. A similar observation of tensile properties was reported for chitosan/PVA/GO electro-spun mats which validates the present research work [26].

Table 6.2 Physical and mechanical properties of the nanofiber mats

Films	Nanofiber diameter (nm)	Nanofiber mat thickness (mm)	TS (MPa)	EAB (%)	WVP × 10^{-5} (g/m.hr.P)	MRC (%)	WCA
P_6	116.27 ±37.64	0.158 ±0.001^{a}	11.36 ±0.26^{a}	26.82 ±0.29^{a}	1.049 ±0.048^{a}	95.68 ±0.12^{a}	51.32 ±0.17°^{a}
$P_6C_{0.5}$	90.51 ±17.56	0.156 ±0.001^{b}	13.49 ±0.30^{b}	6.66 ±0.15^{b}	1.034 ±0.005^{ab}	94.22 ±0.27^{b}	49.08 ±0.32°^{b}
$P_6C_{0.5}G_{0.1}$	134.81 ±31.10	0.161 ±0.001^{c}	14.27 ±0.20^{c}	42.02 ±0.24^{c}	0.997 ±0.014^{bc}	91.04 ±0.126^{c}	47.44 ±0.72°^{c}
$P_6C_{0.5}G_{0.3}$	169.22 ±73.54	0.160 ±0.001^{c}	16.64 ±0.25^{d}	38.09 ±0.17^{d}	0.980 ±0.005^{c}	90.84 ±0.04^{c}	45.92 ±0.69°^{d}

Datas are presented as the mean ± standard deviation of triplicate assays. Significant differences ($P \leq 0.05$) were observed among the corresponding columns labelled with letters (a-d).

6.4.5 Thermal analysis

The thermal characteristics of the nanofiber mats were assessed at temperature upto 600 °C by thermogravimetric analysis (TGA), and Derivative Thermogravimetry (DTG) thermographs as illustrated in Figure 6.9 (a) and (b). The illustrated curves show the mass loss percentage and the rate of mass loss at increasing temperatures, providing valuable information on the thermal stability of the nanofiber mats. In Figure 6.9 (a), three stages of mass degradation were observed for PVA and its hybrid nanofiber mats where the initial

mass loss below 100 °C indicates the evaporation of moisture. The second stage mass loss, occurring at temperatures above 200 °C, involves the breakdown or degradation of primary molecular structure and the formation of polyene compounds. While, the third stage observed above 400 °C, indicates the degradation of adjacent chains in polymeric films. However, the final stage of decomposition was attributed to the breakdown of remaining carbonaceous material and ash formation as final residue. Generally, thermal stability of a material is evident in the second stage, while the third stage suggests the material's degradation. During the third phase, thermally unstable materials display a steep decline compared to thermally stable materials [15].

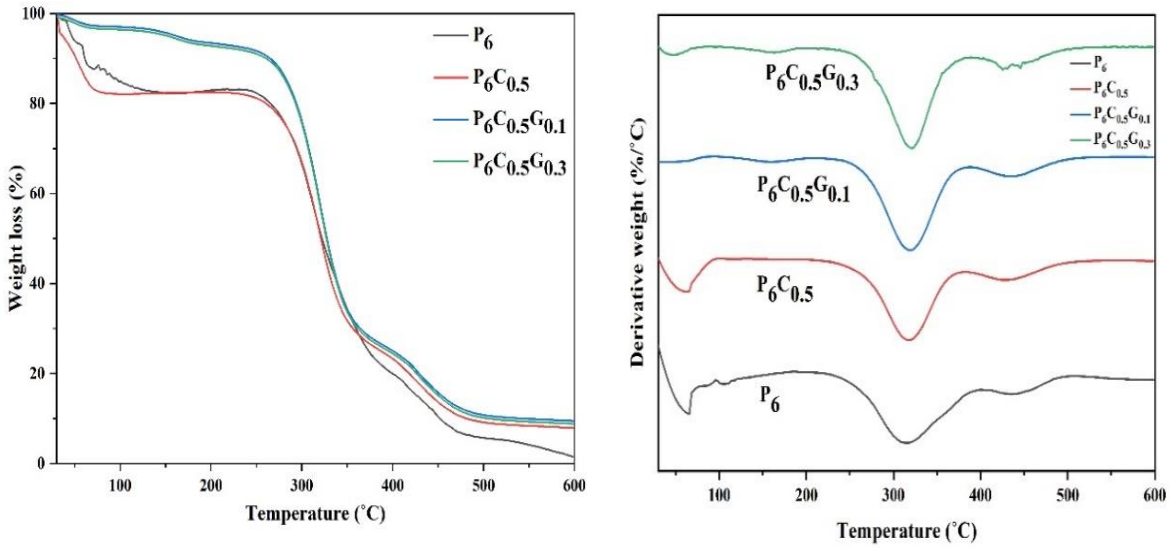

(a) TGA (b) DTG

Figure 6.9 Thermal analysis (a) TGA (b) DTG

For $P_6C_{0.5}$ nanofiber mats, the second step of mass degradation involved the decomposition of the carboxylate group, which is the characteristic of CMC structure. As observed in Figure 6.9 (a), the TGA thermogram of $P_6C_{0.5}$ exhibits minimal weight loss compared to pure PVA due to the improved interfacial interactions and amorphous nature of the polymer blend. Similar type of mass degradation was observed in PVA/CMC/CuO films, where the second and final decomposition was observed at onset temperature between 200 ℃ and 400 ℃ and above 400 ℃ [41]. With the introduction of GO, there is an increase in the degradation temperature with reduced mass loss of $P_6C_{0.5}G_{0.1}$ and $P_6C_{0.5}G_{0.3}$ nanofibers compared to P_6 and $P_6C_{0.5}$ nanofiber mats. The sp^2-hybridized carbon arrangement and large specific surface area of GO facilitated the development of H-bonds with PVA/CMC polymer chains via oxygen-based functional groups of GO [42]. During

pyrolysis, the nanofiber mats undergo thermal degradation, releasing volatile by-products. However, the H-bonding between GO and PVA/CMC required a higher temperature for bond disruption, leading to a reduced degradation rate. Thus, PVA/CMC/GO nanofiber mats displayed increased thermal stability and decreased pyrolysis compared to PVA and PVA/CMC polymer samples.

The DTG plot in Figure 6.9 (b) showed the rate of mass degradation throughout a three-stage breakdown. For P_6 and $P_6C_{0.5}$ samples, the initial mass loss ranged approximately from 15% to 20% within 40 ℃-200 ℃ temperature range as seen from DTG curve. However, with the incorporation of GO, the initial mass loss was reduced to 5%-8% within the 40 ℃-200 ℃ temperature range. The second decomposition stage, characterized by a more substantial mass loss, occurred in the temperature range of 230 ℃-390 °C, accounting for 55%-60% for samples P_6 and $P_6C_{0.5}$. In this stage, the rate of mass loss at the decomposition peak temperature for $P_6C_{0.5}$ is 5%-10% less than the neat PVA sample. However, a significant improvement in thermal degradation was evident in GO-based samples for $P_6C_{0.5}G_{0.1}$ and $P_6C_{0.5}G_{0.3}$, where the maximum mass loss of 60%-65% occurred in the second degradation zone from 250 ℃ to 370 °C. The final decomposition of all samples took place at an offset temperature of 380 ℃-400 °C, where a mass loss of 10%-20% was seen from the TGA curve. The reduction in mass degradation in PVA/CMC/GO samples is due to the improved interaction and presence of an amorphous phase in the hybrid material as compared to neat PVA and PVA/CMC samples. Addition of GO significantly improved thermal stability by reducing dehydration processes and mass loss during pyrolysis, concurrently enhancing nanofiber resistance to heat. A similar pattern in the DTG curve was observed for PVA/GO films with where 50% mass loss occurred at offset temperature of 250 °C, validating the findings of present study [43]. A comparable result was reported, showing the enhanced thermal stability of graphene sheet in PVA/GS films [44]. Thus, integrating graphene-based nanofillers into hybrid polymer systems enhances thermal stability, reduces dehydration processes, and mass loss during calcination. This indicates that GO improves the polymer's ability to withstand high temperatures by increasing its onset temperature and heat resistance.

6.4.6 Water contact angle, water vapor permeability and moisture retention capacity

The wettability of the nanofiber mats is assessed by measuring water contact angles as seen in Table 6.2 and Figure 6.10. It was noted that the WCA of the nanofiber mats ranged from

45.92±0.69° to 51.32±0.17°. P_6 film demonstrated a WCA of 51.32±0.17°, whereas addition of CMC reduced the WCA of sample $P_6C_{0.5}$ to 49.08±0.32°. This showed the increase in the hydrophilic nature of the nanofiber mat with the addition of CMC. Addition of CMC contributes to an elevation in the wettability of nanofiber mats due to the presence of hydrophilic compounds such as -COOH, -OH, and NH_2 [15,45]. Similar findings indicate that the CMC/PVA nanofiber membrane exhibits excellent hydrophilicity and high permeability, making it an ideal substrate material for water purification membranes [46].

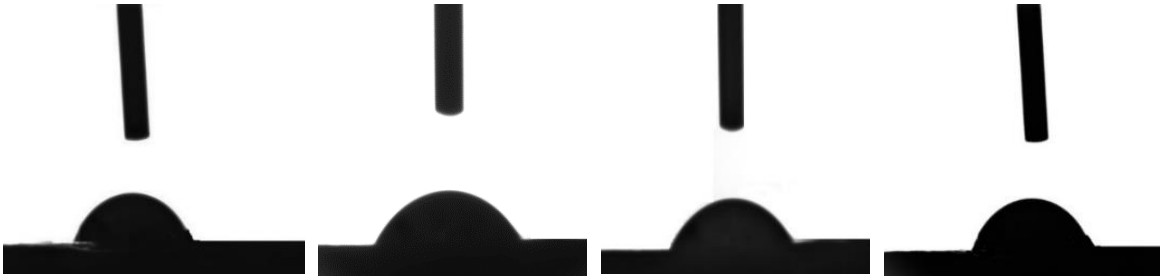

P_6	$P_6C_{0.5}$	$P_6C_{0.5}G_{0.1}$	$P_6C_{0.5}G_{0.3}$
(51.32±0.17°)	(49.08±0.32°)	(47.44±0.72°)	(45.92±0.69°)

Figure 6.10 Contact angle measurement of the developed nanofiber mats

However, incorporating GO (0.1%-0.3%) significantly decreased the WCA of $P_6C_{0.5}G_{0.1}$ and $P_6C_{0.5}G_{0.3}$ nanofiber mats from 47.44 ±0.72° to 45.92±0.69°. Previous studies have demonstrated that uncross-linked PVA nanofibers are predominantly hydrophilic in nature, and exhibits low WCA [15]. The enhanced hydrophilicity observed in the modified GO-based nanofibers which is attributed to the inherent hydrophilic characteristics of PVA/CMC polymer and GO fillers. The existence of numerous oxygen-containing groups, such as carboxyl, hydroxyl, and epoxy, on the GO nanosheets significantly augments the hydrophilicity nanofiber mats. Addition of GO resulted in an increased spacing between fillers, facilitating water penetration into the membranes. Thus, improving surface wettability and reducing the adhesion of hydrophobic pollutants to nanofibers. This is accomplished by the improved hydrophilicity of mats, which produces a protective water barrier between the hydrophilic membrane surface and hydrophobic pollutants, thus preventing their attachment and deposition on the membrane [47,48].

The MRC and WVP of nanofiber mats are crucial factors for packaging plastics in maintaining the quality and extending the shelf life of packaged items over time [30]. A high MRC suggests that the film can retain moisture, which is suitable for packaging

applications where moisture retention is important. Whereas, a lower WVP indicates enhanced barrier efficiency against water vapor transmission, which helps to minimize moisture loss and prevents food dehydration [14]. From Table 6.2, it was seen that sample P_6 has an MRC of 95.68%, whereas with the addition of CMC, the MRC of sample $P_6C_{0.5}$ was found to be 94.22%. While adding GO nanofiller, there was significant change in the MRC from 91.04% to 90.85% ($P_6C_{0.5}G_{0.1}$ and $P_6C_{0.5}G_{0.3}$). The reduction in MRC from $P_6C_{0.5}$ to $P_6C_{0.5}G_{0.1}$ was due to the hydrophilic properties of both PVA/CMC and GO, which trapped the water molecules within the matrix, facilitating the formation of H-bonds [49]. This impend the mobility of polymer chains and the diffusion of water molecules in the nanofiber mats. Studies indicate that the ideal MRC value for food packaging films ranges from 78% to 95% [41,43]. This implies that the MRC of the developed nanofiber mats aligns with the recommended range for food packaging applications, suggesting its capability to hold moisture effectively and prevent its loss, thereby maintaining the quality and extending the shelf life of the packaged food products.

The WVP values of the nanofiber mats, as depicted in Table 6.2, ranged from 0.980 ± 0.005×10^{-5} to 1.049 ± 0.048 $\times10^{-5}$ (g/m.hr.Pa). It was observed that the WVP of P_6 nanofiber mat is 1.049 ± 0.048×10^{-5} (g/m.hr.Pa), whereas for $P_6C_{0.5}$ nanofiber mat it is 1.034± 0.005×10^{-5} (g/m.hr.Pa). However, with the additional GO, the WVP of $P_6C_{0.5}G_{0.1}$ and $P_6C_{0.5}G_{0.3}$ was calculated approximately to 0.997± 0.014×10^{-5} and 0.980± 0.005×10^{-5} (g/m.hr. Pa). Addition of 0.3% GO led to a notable decrease in WVP by 5.22% as compared to $P_6C_{0.5}$. The reduction is attributed to the formation of H-bonds between GO and the PVA/CMC polymer chains thus limiting the availability of -OH groups and restricts the mobility of the polymer chains. This increases the tortuosity of the water molecules, thus impeding their motion within the polymer matrix, which subsequently declined the permeability property of the nanofiber mats. Exceeding the optimal GO concentration led to nanofiller agglomeration and irregular nanofiber development, subsequently increasing its permeability [42]. Thus, the strategic incorporation of GO into the PVA/CMC matrix facilitates the restriction of polymer chain mobility and water vapor diffusion through the nanofiber mats, thereby improving its vapor barrier properties.

6.4.7 FTIR

The FTIR analysis assessed the structural attributes and detect chemical groups and their bonding within the polymer matrix. Neat PVA films displayed a significant absorption peak ranging from 3200 cm^{-1} to 3700 cm^{-1}, associated with symmetric stretching and

vibration of -OH groups as seen in Figure 6.11. Additionally, distinct absorbance peaks at 1033 cm^{-1}, 1382 cm^{-1}, 1466 cm^{-1}, 1645 cm^{-1}, 2927 cm^{-1}, and 3431 cm^{-1} were linked to C-O stretching, C-H vibration, CH_2 bending, H-O-H deformation, -CH_2 stretching, and -OH stretching, respectively [43,50]. For hybrid PVA/CMC sample, change in the absorption peak to a higher wavelength at 1049 cm^{-1}, indicates the interaction between PVA and CMC. Moreover, $P_6C_{0.5}$ sample displayed specific peaks at 1670 cm^{-1} and 1081 cm^{-1}, associated with the stretching of C=O and C-O, respectively [51,52]. The semi-crystalline structure of PVA forms domain influenced by various process parameters, including crosslinking, viscosity, conductivity etc. The interaction between PVA and CMC is evident in a slight shift of the -OH absorption band, indicating intramolecular forces between carboxylate and hydroxyl groups [53]. This shift validates the development of H-bonds with the -OH group in the hybrid polymer system, leading to a narrowing and shifting of the band towards the lower wavenumber, from 3430 cm^{-1} to 3427 cm^{-1}. The FTIR spectra analysis of PVA/CMC/GO films indicate minimal impact on the structure of PVA.

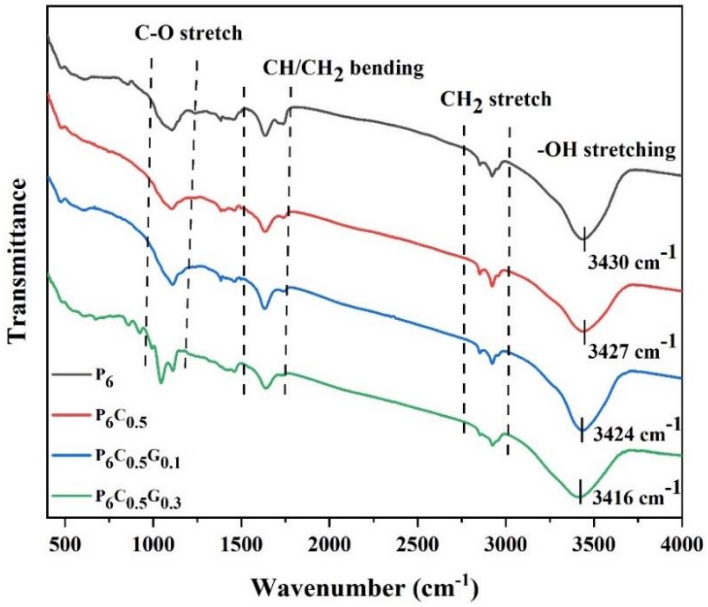

Figure 6.11 FTIR analysis of nanofiber mats

For samples $P_6C_{0.5}G_{0.1}$ and $P_6C_{0.5}G_{0.3}$, the -OH stretching absorption peak shifted to lower wavenumbers, specifically 3434 cm^{-1} and 3416 cm^{-1}, respectively, when GO is added. Addition of GO into the hybrid PVA/CMC polymer solution resulted in the dissociation of H-bonds in the -OH group of the PVA/CMC matrix and forms an additional H-bond with the functional group of GO containing oxygen which is thermodynamically

more favourable. The increase in the concentration of GO nanofiller resulted in H-bond degradation in the -OH groups of the PVA/CMC polymer chain due to increase in conductivity, thus forming an additional H-bond with GO which is an important factor for characteristic intensification [36]. With the increase in GO concentration, degradation of H-bonds in the -OH groups of the polymer chain were observed, resulting in the formation of more H-bonds with GO [54]. This process is a critical factor in enhancing the characteristic intensification of the nanocomposite mats, indicating that the incorporation of GO fosters strong interactions, thereby improving the material's amorphous nature and thermal stability. Thus, the findings emphasize considerable potential of electrospun-derived nanofiber mats from PVA, particularly when incorporating CMC biopolymer and GO nanofillers, to address the development of more sustainable and advanced materials as a feasible substitute for traditional plastics.

6.5 Conclusions

The present study demonstrates successful fabrication of PVA, PVA/CMC, and PVA/CMC/GO nanofiber mats via electrospinning technique. It highlights the impact of incorporating CMC biopolymer and GO nanofiller on the solution properties and the characteristics of the resulting nanofiber mats. Some important findings from the present research work are as follows:

- The incorporation of CMC and GO notably increased the solution conductivity and viscosity, resulting in significant alteration to the nanofiber diameter.
- FESEM study showed that nanofibers derived from PVA and PVA/CMC (6:0.5 w/v) in a 50:50 polymer ratio exhibited a smooth and bead-free structure, showcasing enhanced electrospinning of the polymer solution. Furthermore, incorporation of GO from (0.1 wt.%-0.3 wt.%) in PVA/CMC solution resulted in minimal bead formation in the nanofiber mats with less nanofiller agglomeration.
- Incorporation of CMC and GO significantly improved the tensile properties of PVA nanofiber mats. The addition of 0.5 wt. % CMC led to an 18.696% increase in TS while reducing elongation. Moreover, adding 0.1 wt.%-0.3 wt.% GO nanofillers resulted in rise in TS from 25.59% to 46.41%. These mechanical improvements were attributed to the uniform dispersion of GO within the polymer matrix and enhanced crosslinking within the polymer blends.

- The rheological assessment of the nanofiber solutions demonstrated unique viscoelastic properties, with PVA and PVA/CMC solutions displaying shear thickening behavior, while GO-based PVA/CMC solutions exhibited shear thinning characteristics. Moreover, it also demonstrated enhanced elastic properties for GO induced nanofiber mats, with improvements in storage modulus and shear stress.
- The thermal characteristics showed improvement in the decomposition temperature of PVA/CMC/GO nanofiber mats, accompanied by minimal mass loss compared to PVA and PVA/CMC mats. Moreover, within 200 ℃, the mass loss of GO-based nanofiber was approximately 5%-10% lower as compared to PVA and PVA/CMC mats, showing the potential of GO nanofiber mats in thermal packaging.
- The presence of hydrophilic functional groups increases the wettability of nanofiber mats, as indicated by reduced water contact angles from 51.321° to 45.924°. The oxygen-rich structure of GO enhances the barrier properties of nanofiber mats, resulting in improved WVP from 1.049 to 0.980 (g/m.h. Pa) and MRC from 95.68% to 90.854%. The ideal MRC value for food packaging films ranges from 78% to 95% and the developed nanofiber mats MRC aligns with the recommended range for food packaging applications, suggesting its capability to hold moisture effectively and prevent its loss.
- FTIR spectra confirmed the intermolecular interactions between hydroxyl (-OH) groups of PVA and carboxylate groups (-COOH) of CMCs, with increased intensity in -OH and C-H absorption bands, with GO facilitating new H-bonds within the polymer matrix.

Thus, the study validates the effective use of CMC and GO additives in PVA polymer producing nanofiber mats that exhibit enhanced structural, mechanical, thermal, and barrier properties suitable for packaging applications.

Bibliography

1. Guo, Y., Wang, X., Shen, Y., Dong, K., Shen, L., and Alzalab, A. A. A. Research progress, models and simulation of electrospinning technology: a review. *Journal of Materials Science*, 57:58–104, 2022.

2. Sharma, C., Dhiman, R., Rokana, N., and Panwar, H. Nanotechnology: an untapped resource for food packaging. *Frontiers in Microbiology*, 8:243298, 2017.

3. Siskova, A. O., Frajova, J., and Nosko, M. Recycling of poly(ethylene terephthalate) by electrospinning to enhanced the filtration efficiency. *Materials Letters*, 278:128426, 2020.

4. Tcharkhtchi, A., Abbasnezhad, N., Seydani, M. Z., Zirak, N., Farzaneh, S., and Shirinbayan, M. An overview of filtration efficiency through the masks: Mechanisms of the aerosols penetration. *Bioactive Materials*, 6:106–122, 2021.

5. Zhang, W., He, Z., Han, Y., Jiang, Q., Zhan, C., Zhang, K., Li, Z., and Zhang, R. Structural design and environmental applications of electrospun nanofibers. *Composites Part A: Applied Science and Manufacturing*, 137:106009, 2020.

6. Aliheidari, N., Aliahmad, N., Agarwal, M., and Dalir, H. Electrospun nanofibers for label-free sensor applications. *Sensors*, 19(16):3587, 2019.

7. Yılmaz, S. S. and Aytac, A. Development of cross-linked polyvinyl alcohol/sodium caseinate/silver nanoparticle electrospun mats for antibacterial wound dressing. *Journal of Vinyl and Additive Technology*, 30(4):911–928, 2014.

8. Kumar, T. S. M., Kumar, K. S., Rajini, N., Siengchin, S., Ayrilmis, N., and Rajulu, A. V. A comprehensive review of electrospun nanofibers: Food and packaging perspective. *Composites Part B: Engineering*, 175:107074, 2019.

9. Ura, D. P. and Stachewicz, U. Direct electrospinning of short polymer fibers: factors affecting size and quality. *Composites Part A: Applied Science and Manufacturing*, 181:108138, 2024.

10. Ji, W., Zhao, G., Guo, C., Fan, L., Deng, H., Du, R., Fu, M., Sui, G., and Fu, Q. A novel method to fabricate two-dimensional nanomaterial based on electrospinning. *Composites Part A: Applied Science and Manufacturing*, 143:106275, 2021.

11. Erbay, E. A., Yeşilsu, A. F., and Türe, M. Fish gelatin antimicrobial electrospun nanofibers for active food-packaging applications. *Journal of Nano Research*, 56:80–97, 2019.

12. Zhang, M., Ahmed, A., and Xu, L. Electrospun Nanofibers for functional food packaging application. *Materials*, 16(17):5937, 2023.

13. Xu, C., Shi, L., Guo, L., Wang, X., Wang, X., and Lian, H. Fabrication and characteristics of graphene oxide/nanocellulose fiber/poly(vinyl alcohol) film. *Journal of Applied Polymer Science*, 134(39): 45345, 2017.

14. Sarwar, M. S., Niazi, M. B. K., Jahan, Z., Ahmad, T., and Hussain, A. Preparation and characterization of PVA/nanocellulose/Ag nanocomposite films for antimicrobial food packaging. *Carbohydrate Polymers*, 184:453–464, 2018.

15. Hashmi, M., Ullah, S., Ullah, A., Saito, Y., Haider, M. K., Bie, X., Wada, K., and Kim, I. S. Carboxymethyl cellulose (CMC) based electrospun composite nanofiber mats for food packaging. *Polymers*, 13(2):302, 2021.

16. Das, P., Ojah, N., Kandimalla, R., Mohan, K., Gogoi, D., Dolui, S. K., and Choudhury, A. J. Surface modification of electrospun PVA/chitosan nanofibers by dielectric barrier discharge plasma at atmospheric pressure and studies of their mechanical properties and biocompatibility. *International Journal of Biological Macromolecules*, 114:1026–1032, 2018.

17. Huang, C. L., Peng, S. Y., Wang, Y. J., Chen, W. C., and Lin, J. H. Microstructure and characterization of electrospun poly(vinyl alcohol) nanofiber scaffolds filled with graphene nanosheets. *Journal of Applied Polymer Science*, 132(17):41891, 2015.

18. Yu, G., Li, T. S., Xu, M., Andersson, M., Li, B., Tang, H., Parbey, J., and Shao, J. Fabrication of nickel-YSZ cermet nanofibers via electrospinning. *Journal of Alloys and Compounds*, 693:1214–1219, 2017.

19. Allafchian, A., Hosseini, H., and Ghoreishi, S. M. Electrospinning of PVA-carboxymethyl cellulose nanofibers for flufenamic acid drug delivery. *International Journal of Biological Macromolecules*, 163:1780–1786, 2020.

20. Qiao, Z., Gu, J., Zuo, Y., Tan, H., and Zhang, Y. The effect of carboxymethyl cellulose addition on the properties of starch-based wood adhesive. *BioResources*, 9(4):6117–6129, 2014.

21. Ginestra, P., Riva, L., Fiorentino, A., Zappa, D., Comini, E., and Ceretti, E. Electrospinning of poly(vinyl alcohol)-graphene oxide aligned fibers. *Procedia CIRP*, 89:110–115, 2020.

22. Huang, C. L., Lee, K. M., Liu, Z. X., Lai, R. Y., Chen, C. K., Chen, W. C., and Hsu, J. F. Antimicrobial activity of electrospun polyvinyl alcohol nanofibers filled with poly[2-(tert-butylaminoethyl) methacrylate]-grafted graphene oxide nanosheets. *Polymers*, 12(7):1449, 2020.

23. Aguero, L. E. M., Saul, C. K., De Freitas, R. A., Duarte, M. E. R., and Noseda, M. D. Electrospinning of marine polysaccharides: processing and chemical aspects, challenges, and future prospects. *Nanotechnology Reviews*, 11:3250–3280, 2022.

24. Sharma, B. Viscoelastic investigation of graphene oxide grafted PVA biohybrid using ostwald modeling for packaging applications. *Polymer Testing*, 91:106791, 2020.

25. Huang, C. L., Wu, H. H., Jeng, Y. C., and Liang, W. Z. Electrospun graphene nanosheet

-filled poly(trimethylene terephthalate) composite fibers: effects of the graphene nanosheet content on morphologies, electrical conductivity, crystallization behavior, and mechanical properties. *Polymers*, 11:164, 2019.

26. Yang, S., Liu, Y., Jiang, Z., Gu, J., and Zhang, D. Thermal and mechanical performance of electrospun chitosan/poly(vinyl alcohol) nanofibers with graphene oxide. *Advanced Composites and Hybrid Materials*, 1:722–730, 2018.

27. Ekrami, E., Khodabandeh Shahraky, M., Mahmoudifard, M., Mirtaleb, M. S., and Shariati, P. Biomedical applications of electrospun nanofibers in industrial world: a review. *International Journal of Polymeric Materials and Polymeric Biomaterials*, 72(7):561–575, 2023.

28. Chen, C. H., Kuo, W. S., and Lai, L. S. Rheological and physical characterization of film-forming solutions and edible films from tapioca starch/decolorized hsian-tsao leaf gum. *Food Hydrocolloids*, 23(8):2132–2140, 2009.

29. Ma, Q., Du, L., Yang, Y., and Wang, L. Rheology of film-forming solutions and physical properties of tara gum film reinforced with polyvinyl alcohol (PVA). *Food Hydrocolloids*, 63:677–684, 2017.

30. Meree, C. E., Schueneman, G. T., Meredith, J. C., and Shofner, M. L. Rheological behavior of highly loaded cellulose nanocrystal/poly(vinyl alcohol) composite suspensions. *Cellulose*, 23(5):3001–3012, 2016.

31. Shekhar, S., Sharma, R., Sharma, S., Sharma, B., Sarkar, A., and Jain, P. An exploration of electrocatalytic analysis and antibacterial efficacy of electrically conductive poly (d-glucosamine)/graphene oxide bionanohybrid. *Carbohydrate Polymers*, 240:116242, 2020.

32. Bhasha Sharma, Malik, P., and Jain, P. To study the effect of processing conditions on structural and mechanical characterization of graphite and graphene oxide-reinforced PVA nanocomposite. *Polymer Bulletin*, 76(8):3841–3855, 2019.

33. Bouhfid, R., Essabir, H., and Qaiss, A. K. Graphene-based nanocomposites: mechanical, thermal, electrical, and rheological properties. In Thomas, S., Muller, R., and Abraham, J., editors, *Rheology and Processing of Polymer Nanocomposites*, pages 405–430, ISBN:9781118969793, John Wiley & Sons, 2016.

34. Lewandowska, K. and Szulc, M. Rheological and mechanical studies of chitosan blends with the addition of an ionic liquid. *Progress on Chemistry and Application of Chitin and its Derivatives*, 24:119-126, 2019.

35. Schramm, G. *A practical approach to rheology and rheometry*. Gebrueder Haake, Karlsruhe, Federal Republic of Germany, 2nd edition, 1994.

36. Huang, C. L., Peng, S. Y., Wang, Y. J., Chen, W. C., and Lin, J. H. Microstructure and characterization of electrospun poly(vinyl alcohol) nanofiber scaffolds filled with graphene nanosheets. *Journal of Applied Polymer Science*, 132(17):41891, 2015.

37. Wu, S., Li, K., Shi, W., and Cai, J. Preparation and performance evaluation of chitosan/ polyvinylpyrrolidone/polyvinyl alcohol electrospun nanofiber membrane for heavy metal ions and organic pollutants removal. *International Journal of Biological Macromolecules*, 210:76–84, 2022.

38. Wu, S., Shi, W., Li, K., Cai, J., Xu, C., Gao, L., Lu, J., and Ding, F. Chitosan-based hollow nanofiber membranes with polyvinylpyrrolidone and polyvinyl alcohol for efficient removal and filtration of organic dyes and heavy metals. *International Journal of Biological Macromolecules*, 239:124264, 2023.

39. Panova, T. V., Efimova, A. A., Berkovich, A. K., and Efimov, A. V. Plasticity control of poly(vinyl alcohol)–graphene oxide nanocomposites. *RSC Advances*, 10(40):24027–24036, 2020.

40. Mangal, R., Srivastava, S., and Archer, L. A. Phase stability and dynamics of entangled polymer–nanoparticle composites. *Nature Communications*, 6:1–9, 2015.

41. Amaregouda, Y., Kamanna, K., and Gasti, T. Biodegradable polyvinyl alcohol/carboxymethyl cellulose composite incorporated with l-alanine functionalized MgO nanoplates: physico-chemical and food packaging features. *Journal of Inorganic and Organometallic Polymers and Materials*, 32(6):2040–2055, 2022.

42. Kapila, K., Kirtania, S., Nath, K. K., Saikumar, A., Badwaik, L. S., and Ahmed, G. A. Synergistic effect of graphene oxide on the properties of poly (vinyl alcohol)/carboxymethyl cellulose electrospun nanofiber mats. *Journal of Vinyl and Additive Technology*, 2025. 31(3):572-588, 2025.

43. Kapila, K., Kirtania, S., Devi, L. M., Saikumar, A., Badwaik, L. S., and Rather, M. A. Potential perspectives on the use of poly (vinyl alcohol)/graphene oxide nanocomposite films and its characterization. *Journal of Food Measurement and Characterization*, 18(2):1012–1025, 2024.

44. Cobos, M., Fernandez, M. J., and Fernández, M. D. Graphene based poly(vinyl alcohol) nanocomposites prepared by in situ green reduction of graphene oxide by ascorbic acid: influence of graphene content and glycerol plasticizer on properties. *Nanomaterials*, 8(12):1013, 2018.

45. Shi, W., Cai, J., Yang, Y., Xu, C., Lu, J., and Wu, S. Electrospun carboxymethyl cellulose/polyvinyl alcohol nanofiber membranes for enhanced metal ion removal.

Sustainability, 15(14):11331, 2023.

46. Hashmi, M., Ullah, S., Ullah, A., Akmal, M., Saito, Y., Hussain, N., Ren, X., and Kim, I. S. Optimized loading of carboxymethyl cellulose (CMC) in tri-component electrospun nanofibers having uniform morphology. *Polymers*, 12(11):2524, 2020.

47. Verma, K., Siddiki, S. H., Maity, C. K., Mishra, R. K., and Moniruzzaman, M. Development of reduced graphene oxide (rGO) reinforced poly(lactic) acid/ cellulose nanocrystal composite through melt mixing: Effect of nanofiller on thermal, structural, biodegradation and antibacterial properties. *Industrial Crops and Products*, 204:117307, 2023.

48. Yang, M., Shi, J., and Xia, Y. Effect of SiO_2, PVA and glycerol concentrations on chemical and mechanical properties of alginate-based films. *International Journal of Biological Macromolecules*, 107:2686–2694, 2018.

49. Akther, N., Ali, S. M., Phuntsho, S., and Shon, H. Surface modification of thin-film composite forward osmosis membranes with polyvinyl alcohol–graphene oxide composite hydrogels for antifouling properties. *Desalination*, 491:114591, 2020.

50. Ma, J., Li, Y., Yin, X., Xu, Y., Yue, J., Bao, J., and Zhou, T. Poly(vinyl alcohol)/graphene oxide nanocomposites prepared by in situ polymerization with enhanced mechanical properties and water vapor barrier properties. *RSC Advances*, 6(55):49448–49458, 2016.

51. Wu, S., Li, K., Shi, W., and Cai, J. Chitosan/polyvinylpyrrolidone/polyvinyl alcohol/carbon nanotubes dual layers nanofibrous membrane constructed by electrospinning-electrospray for water purification. *Carbohydrate Polymers*, 294:119756, 2022.

52. Dogan, H. Y., Altin, Y., and Bedeloglu, A. C. Fabrication and properties of graphene oxide and reduced graphene oxide reinforced Poly(Vinyl alcohol) nanocomposite films for packaging applications. *Polymers and Polymer Composites*, 30:1-11, 2022.

53. Goswami, A., Bajpai, A. K., Bajpai, J., and Sinha, B. K. Designing vanadium pentoxide-carboxymethyl cellulose/polyvinyl alcohol-based bionanocomposite films and study of their structure, topography, mechanical, electrical and optical behavior. *Polymer Bulletin*, 75(2):781–807, 2018.

54. Bao, C., Guo, Y., Song, L., and Hu, Y. Poly(vinyl alcohol) nanocomposites based on graphene and graphite oxide: a comparative investigation of property and mechanism. *Journal of Materials Chemistry*, 21(36):13942–13950, 2011.